Characterization of the Extra-Large-Pore Zeolite UTD-1

Raul F. Lobo,*,† Michael Tsapatsis,‡ Clemens C. Freyhardt,§,|| Shervin Khodabandeh,§ Paul Wagner,§ Cong-Yan Chen,⊥ Kenneth J. Balkus Jr.,¶ Stacey I. Zones,⊥ and Mark E. Davis*,§

Contribution from the Center for Catalytic Science and Technology, Department of Chemical Engineering, University of Delaware, Newark, Delaware 19716, Division of Chemistry and Chemical Engineering, California Institute of Technology, Pasadena, California 91125, Department of Chemical Engineering, University of Massachusetts, Amherst, Massachusetts 01003, Chevron Research and Technology Co., Richmond, California 94802, and Department of Chemistry, University of Texas at Dallas, Richardson, Texas 75083

Received March 17, 1997[⊗]

Abstract: The molecular sieve UTD-1 is investigated using scanning and transmission electron microscopies (TEM), solid-state NMR spectroscopy, electron (ED) and X-ray diffraction (XRD), adsorption studies, and catalytic test reactions. The results confirm that UTD-1 is the first high-silica zeolite to contain a one-dimensional, extra-large 14-ring pore system. TEM and ED show that UTD-1 is faulted along the (002) planes. Simulations of XRD patterns of faulted structures using DIFFaX indicate that the XRD pattern of a framework containing the so-called double crankshaft chains is in better agreement with the experimental pattern than a framework with the narsarsukite chains previously reported. Thermal/hydrothermal stability studies show that UTD-1 has similar stability to other medium- and large-pore, high-silica zeolites. The ratio of isomerization to disproportionation, and the distribution of trimethylbenzene isomers in the *m*-xylene isomerization test reaction from UTD-1 are similar to those obtained from other large-pore zeolites (zeolites Y or L). However, UTD-1 shows a *p*-/*o*-xylene ratio of products below one.

Introduction

New zeolitic materials offer opportunities to expand the range of industrial applications of microporous materials, provided they contain previously unobserved properties for which novel catalytic reaction selectivity can be expected.[1] Several zeolites with novel pore architectures have been synthesized during the last decade, and include materials with cavities containing 10- and 12-ring windows (NU-87, SSZ-37, SSZ-26, SSZ-33, CIT-1, MCM-22, and SSZ-25).[2−7] An example of how each material type affects the reaction activity, deactivation, and selectivity for the conversion of *m*-xylene has been reported.[8] One of the most sought-after characteristics in zeolitic materials, extra-large pores—pores bounded by more than 12-tetrahedral atoms—has eluded synthetic zeolite science until recently. The synthesis and characterization of the zeolite UTD-1 (University of Texas at Dallas, number 1) have recently appeared.[9−11] Freyhardt et al. demonstrated that UTD-1 is the first high-silica zeolite with extra-large pores.[12] UTD-1 opens potential avenues to important catalysts in the fine chemicals and pharmaceutical industry, in which it is often found that other zeolites cannot be utilized because the organic reactants cannot diffuse inside the smaller pores. The large pores of UTD-1 also provide an opportunity for solid-acid catalysis of large molecular weight hydrocarbons in the petrochemical industry, e.g., the cracking of heavier fractions of the feedstocks in the fluid catalytic cracking units.

UTD-1 is a one-dimensional pore zeolite with pores bounded by 14 tetrahedral (T) atoms (14MR) with an open diameter of approximately 10 × 7.5 Å. Analyses of the X-ray powder diffraction data indicate that UTD-1 is an intergrowth of two or more closely related polymorphs. The structure of UTD-1 can be viewed, in a two dimensional projection, as being formed of layers of two 5-rings connected by 4-rings ($5^2 4^1$ layers parallel to the *ab* plane) as indicated in Scheme 1. Consecutive stackings of these layers create the three-dimensional crystal structure.

Numerous phosphate-based molecular sieves have been synthesized with pores larger than 12-T-atom rings (12MR),[13] starting with VPI-5 in 1988 (18MR)[14] and shortly after followed

* Correspondence: Raul F. Lobo, Center for Catalytic Science and Technology, Department of Chemical Engineering, University of Delaware, Newark, DE. Fax: (302) 831−2085. E mail: lobo@che.udel.edu. Mark E. Davis, Division of Chemistry and Chemical Engineering, 210-41, California Institute of Technology, Pasadena, CA 91125.

|| Current address: Solid State Chemistry, Department of Chemistry, University of Constance, University Street 10, D-78434, Constance, Germany.

⊥ Chevron Research and Technology.

¶ University of Texas at Dallas.

† University of Delaware.

‡ University of Massachusetts.

§ California Institute of Technology.

⊗ Abstract published in *Advance ACS Abstracts,* August 15, 1997.

(1) Davis, M. E. *Chem. Ind.* **1992**, 137.

(2) Shannon, M. D.; Casci, J. L.; Cox, P. A.; Andrews, S. J. *Nature* **1991**, *353*, 417−420.

(3) Nakagawa, Y. *Stud. Surf. Sci. Catal.* **1994**, *84*, 323−330.

(4) Zones, S. I.; Olmstead, M. M.; Santilli, D. S. *J. Am. Chem. Soc.* **1992**, *114*, 4195−4201.

(5) Lobo, R. F.; Davis, M. E. *J. Am. Chem. Soc.* **1995**, *117*, 3764−3779.

(6) (a) Leonowicz, M. E.; Lawton, J. A.; Lawton, S. L.; Rubin, M. K. *Science* **1994**, *264*, 1910−1913. (b) Chan, I. Y.; Labun, P. A.; Pan, M.; Zones, S. I. *Microporous Mater.* **1995**, 3, 409−418.

(7) Rasband, W., *NIH Image*, Nat. Inst. Health: Bethesda, MD **1996**; version 1.60.

(8) Adair, B.; Chen, C. Y.; Wan, K. T.; Davis, M. E. *Microporous Mater.* **1996**, *7*, 261−270.

(9) Balkus, K. J.; Gabrielov, A. G.; Sandler, N. *Mater. Res. Soc. Symp. Proc.* **1995**, *368*, 369−375.

(10) Balkus, K. J.; Khanmamedova, A.; Gabrierlov, A. G.; Zones, S. I. *Stud. Surf. Sci. Catal.* **1996**, *101*, 1341−1348.

(11) Balkus, K. J.; Gabrielov, A. G. Synthesis of novel molecular sieves using a metal complex as template. U.S., 5,489,424, 1996.

(12) Freyhardt, C. C.; Tsapatsis, M.; Lobo, R. F.; Balkus, K. J.; Davis, M. E. *Nature* **1996**, *381*, 295−298.

(13) Meier, W. M.; Olson, D. H.; Baerlocher, C. *Atlas of Zeolite Structure Types*, 4th ed.; Elsevier: London, 1996.

(14) Davis, M. E.; Saldarriaga, C.; Montes, C.; Garces, J.; Crowder, C. *Nature* **1988**, *331*, 698−699.

S0002-7863(97)00852-4 CCC: $14.00 © 1997 American Chemical Society

Scheme 1

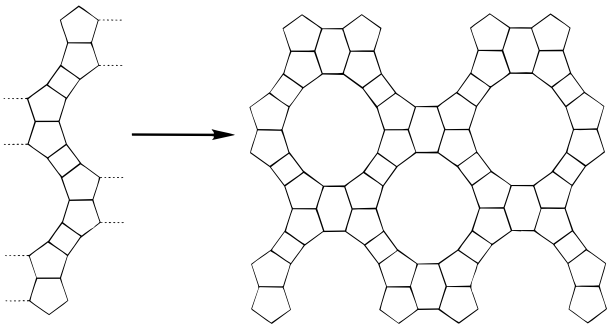

by $AlPO_4$-8 (14MR),[15] cloverite (20MR),[16] JDF-20 (20MR),[17] ULM-5 (16MR),[18] ULM-16 (16MR),[19] and two new vanadium phosphates with 24MR cages.[20,21] However, the practical application of these phosphate-based, extra-large-pore materials has been hampered by their poor thermal and/or hydrothermal stability. UTD-1, on the other hand, shows the typical high thermal and hydrothermal stability of high-silica zeolites.[12]

Because UTD-1 is the first extra-large-pore zeolite, detailed investigation of its physicochemical properties are merited. Here we present a detailed characterization of UTD-1 using synchrotron X-ray powder diffraction, electron diffraction, high-resolution transmission electron microscopy, scanning electron microscopy, solid-state NMR spectroscopy, adsorption studies, and thermal/hydrothermal stability investigations. The relationship between the geometry of the structure-directing agent (bis(pentamethylcyclopentadienyl)cobalt(III)), $[(Cp^*)_2Co]^+$, and the shape and size of the pores is investigated using energy minimization calculations. The acid-catalyzed properties of UTD-1 are investigated using the isomerization of xylenes as a test reaction.

Experimental Section

Synthesis. The samples of UTD-1 were synthesized as previously reported,[12,9] using bis(pentamethylcyclopentadienyl)cobalt(III) hydroxide, $(Cp^*)_2Co$ OH, as a structure-directing agent.[22]

To eliminate the organometallic structure-directing agent from the pores, the as-made UTD-1 (yellow) was heated in a furnace in flowing nitrogen containing a few percent of air. The solid was heated at 1 °C min^{-1} to 540 °C and maintained at this temperature for 4 h; the temperature was increased again at 0.5 °C min^{-1} to 600 °C, and held at this temperature for another 4 h. Finally, the sample was cooled to room temperature over several hours in the furnace. The product has a blue color at this point. After the calcination step, the product contains cobalt oxide occluded in the pores and in the external surface of the crystals (see below). This oxide is eliminated by an aqueous acid treatment (12 N HCl and then 7 N HCl) as previously reported.[12] The samples used here for adsorption studies, X-ray powder diffraction, electron microscopy, and NMR spectroscopy have been treated in this manner before characterization.

For the catalytic tests, the incorporation of aluminum in the samples was carried out as follows: A sample of UTD-1 was prepared using the methods described in ref 23 and calcined as above. Calcined UTD-1 (2.61 g) was suspended in 175 mL water in a polypropylene bottle. A total of 3.48 g of aluminum nitrate nonahydrate was dissolved into the slurry, and the solution was heated for 2.5 days at 90 °C. Upon removing the plastic bottle from the oven, the solution is pink (dissolved cobalt in acidic solution) and the solids are white. The solids are filtered, washed with 100 mL of 0.01 N HCl, and washed with distilled water. Chemical analyses show a SiO_2/Al_2O_3 ratio ~70. The aluminum-containing samples of UTD-1 will be denoted Al-UTD-1.

Analytical. Synchrotron X-ray diffraction data were obtained at the X7A beam line of the Synchrotron Light Source, Brookhaven National Laboratory. The sample, after calcination and removal of the cobalt oxide by acid treatment, was dried at 200 °C for 12 h and packed in a 1 mm glass capillary. The data were collected at room temperature from 2−65° 2θ with a step scan of 0.01° and a wavelength $\lambda = 1.2513$ Å. Room temperature powder X-ray diffraction (XRD) patterns were recorded on a Scintag XDS 2000 diffractometer equipped with a liquid nitrogen-cooled germanium detector, Cu Kα radiation $\lambda = 1.54184$ Å and a Bragg−Brentano geometry.

The thermal and hydrothermal stability of UTD-1 were investigated by *in situ* X-ray powder diffraction. The samples were mounted as thin films on a platinum−rhodium alloy sample-holder/strip-heater within an Edmund Buhler high-temperature XRD chamber. The chamber was evacuated and refilled with the flow gas three times prior to establishing the steady flow under which the data were collected. The flow gas for the thermal stability experiments was dry nitrogen. Nitrogen gas, bubbled through distilled water maintained at room temperature, was used for the hydrothermal experiments. The gas flow rates were approximately 0.5 L min^{-1}. The temperature controller was calibrated to within 10 °C using the melting points of NaCl and KNO_3 as the standards. Samples of calcined and HCl-washed UTD-1 were mounted on the sample holder in thicknesses varying from approximately 0.5 mm to 1 mm. The diffraction scans were taken from 2−51° 2θ with a 0.04 step size and 5 s count periods. In both thermal and the hydrothermal experiments, the temperature was ramped at 10 °C min^{-1}, and held at the designated temperature for 15 min before the scan. X-ray diffraction patterns were recorded at room temperature, 200, 400, 500, 600, 800, 900, 1000 °C and finally again at room temperature.

Scanning electron microscopy (SEM) images were recorded on a Camscan 2-LV electron microscope operating with an acceleration voltage of 15 kV. Thermogravimetric analysis (TGA) was carried out on a Du Pont 951 thermogravimetric analyzer in flowing dry argon using a constant heating rate of 1 K min^{-1}. Chemical composition analyses were carried out at Galbraith Laboratories, Knoxville, TN.

The adsorption capacities of UTD-1, SSZ-24, zeolite L, and zeolite Y were measured at room temperature using a Cahn C-2000 balance coupled with a computer via an ATI-Cahn digital interface. Several "plug gauge" molecules with various kinetic diameters are used.[24] The adsorbate vapors are delivered from the liquid phase and the partial pressure P/P_0 (= 0.15−0.4) of the organic adsorbate was adjusted using a temperature controlled thermostat. Prior to the adsorption experiment, the calcined samples are dehydrated at 615 K under a vacuum of 10^{-3} Torr for 5 h. The pore volumes are given on the basis of the weight gains of the adsorbents upon adsorption, and the densities of the liquid adsorbates at room temperature, i.e., assuming that the adsorbates in the sample pores have the same density as the liquid state.

Solid-state NMR spectroscopy was performed on a Bruker AM 300 spectrometer equipped with a high power assembly for solids. Samples were packed into 4 and 7 mm ZrO_2 rotors and spun in air. ^{29}Si NMR (59.63 MHz) single-pulse experiments were performed at spinning rates of 2.7−3.5 kHz, pulse widths of 4 μs (40° pulse), and recycle delays of 10−100 s. ^1H-^{29}Si CPMAS NMR spectra were measured with ^1H decoupling at spinning rates of 2.5−3 kHz using a 7 ms ^1H pulse (^1H 90°), ^{29}Si contact times of 5−15 ms, and recycle times of 3 s. ^{29}Si NMR chemical shifts are referenced to external standard of tetrakis(trimethylsilyl)silane (downfield resonance at −10.05 ppm relative to tetramethylsilane). ^1H NMR (300.15 MHz) spectra were measured at

(15) Dessau, R. M.; Schlenker, J. L.; Higgins, J. B. *Zeolites* **1990**, *10*, 522−524.
(16) Estermann, M.; McCusker, L. B.; Baerlocher, C.; Merrouch, A.; Kessler, H. *Nature* **1991**, *352*, 320−323.
(17) Jones, R. H.; Thomas, J. M.; Chen, J. S.; Xu, R. R.; Huo, Q. S.; Li, S. G.; Ma, Z. *J. Solid State Chem.* **1993**, *102*, 202−208.
(18) Loiseau, T.; Ferey, G. *J. Solid State Chem.* **1994**, *111*, 403−415.
(19) Loiseau, T.; Ferey, G. *J. Mater. Chem.* **1996**, *6*, 1073−1074.
(20) Khan, M. I.; Meyer, L. M.; Haushalter, R. C. *Chem. Mater.* **1996**, *8*, 43−53.
(21) Schindler, M.; Joswig, W.; Baur, W. H. *Z. Anorg. Allg. Chem.* **1997**, *623*, 45−54.
(22) Balkus, K. J.; Gabrielov, A. G.; Zones, S. I.; Chan, I. Y. In *Synthesis of Microporous Materials, Zeolites, Clays and Nanocomposites*; Kessler, H., Occelli, M., Eds.; Marcel Dekker: New York, 1996.
(23) Zones, S. I.; Nakagawa, Y. *Microporous Mater.* **1994**, *2*, 543−555.
(24) Breck, D. W. *Zeolite Molecular Sieves: Structure, Chemistry and Use*; Wiley: New York, 1974.

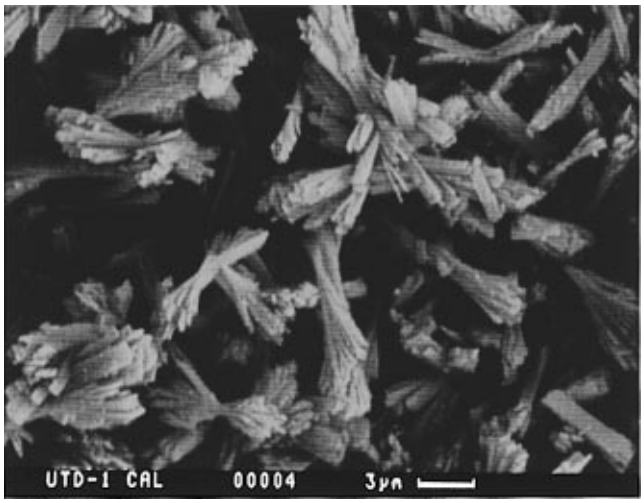

Figure 1. Scanning electron micrograph of a sample of as-synthesized UTD-1.

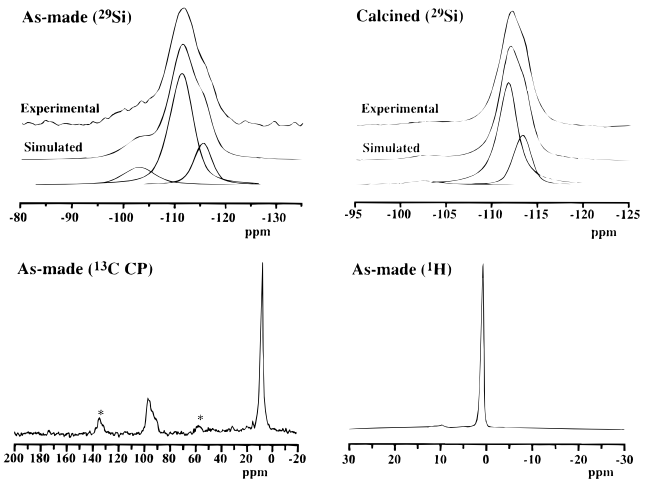

Figure 2. Solid-state NMR spectra of UTD-1: (a) ^{29}Si MAS NMR spectrum of as-made UTD-1; (b) ^{29}Si MAS NMR spectrum of a calcined sample; (c) ^{13}C CP/MAS of the as-made sample; and (d) ^{1}H MAS NMR of as-made UTD-1. An asterisk (*) indicates a spinning side band.

a spinning rate of 11 kHz, pulse lengths of 6.2 μs (70° pulse), and delay times of 5 s. ^{1}H NMR chemical shifts are referenced to adamantane (δ = 1.74 ppm vs TMS). ^{13}C NMR (75.47 MHz) spectra were measured using cross-polarization with a ^{1}H 90° pulse of 7 μs and a contact time of 10 ms at spinning rates of 2.6 kHz, ^{13}C NMR chemical shifts are referenced to adamantane (downfield resonance at 38.4 relative to TMS). Exponential line broadening of 30 Hz was applied to ^{29}Si and ^{13}C NMR data, and spectral fitting was performed using Bruker LINESIM software and QNMR software.

The samples for transmission electron microscopy (TEM) are prepared by both direct dispersing and microtomy. For direct dispersion, a drop of the zeolite suspension in ethanol is transferred to a carbon-coated Cu grid. For microtomy, the samples are first embedded in epoxy (LR white) by vacuum impregnation followed by heating at 90 °C for 2 h. Sections are prepared using a diamond knife mounted on an ultramicrotome. Thin sections are collected on a carbon-coated Cu grid. The sample grids are allowed to dry at 110 °C under vacuum overnight before mounting on the microscope specimen holder. Electron diffraction, transmission electron microscopy, and high-resolution electron microscopy (HREM) were performed on a Phillips 430 microscope operated at 200 kV. Image processing was carried out using the "Image" software for the MacIntosh.[7]

Molecular dynamics and energy minimization calculations were carried out using CERIUS^2 (v 2.0) of MSI Inc. The UFF force field of Rappe et al.[25] was used in all the calculations.

m-Xylene isomerization reactions were carried out in a fixed-bed reactor at 317 °C (controlled within 1 °C) and ambient pressure. A total of 53 mg of Al-UTD-1 in its acid form was activated under flowing He by heating to 350 °C with a temperature ramping rate of 1.2 °C min^{-1} and maintained at 350 °C for 4 h. After activation of the sample, the He gas inlet was passed through a saturator filled with *m*-xylene (Aldrich 99+%) adsorbed on Chromosorb 102 (Supelco, Bellefonte, Pa) at 10 °C ($P_{m\text{-xylene}}$ = 3.4 Torr). All inlet/outlet lines were heated to at least 120 °C to prevent condensation within the lines. The outlet of the reactor was analyzed by on-line gas chromatography (HP5890 series II equipped with a 25 m HP-FFAP column and flame ionization detector).

Results and Discussion

As-synthesized UTD-1 is a yellow powder, suggesting that the organometallic structure-directing agent (also yellow) is occluded intact inside the void space of the material. UV diffuse-reflectance spectra of the organometallic complex, alone and in UTD-1, are identical confirming the previous statement.[22] SEM of the as-synthesized zeolite (Figure 1) shows that UTD-1 crystallizes in long platelike crystals with approximate dimensions of 1 μm by 5 μm. Only one morphology is observed in the micrograph, an indication that no other phases are present in the sample besides UTD-1. The SEMs of the calcined and acid treated UTD-1, i.e., cobalt free, are also indistinguishable from the as-synthesized material, suggesting that this zeolite is thermally stable and resistant to the aqueous acid environments used to eliminate the cobalt oxide formed during calcination.

NMR Spectroscopy. As previously reported, the structure of UTD-1 is a fully connected framework of tetrahedral $TO_{4/2}$ oxide units.[12] The structure is highly faulted and due to the positive charge of the organometallic complex, in agreement with reports for other high-silica zeolites,[26−31] the presence of large numbers of internal silanol groups is observed.[31] The results from ^{29}Si NMR and ^{1}H-^{29}Si CP/MAS NMR spectroscopy of the as-synthesized material show the presence of silicon Q^3 for the as-made sample (Q^n stands for $X_{4-n}Si[OSi]_n$, X = OH or O$^-$), with a relative population of approximately 10% [$Q^3/(Q^3 + Q^4)$] (see Figure 2a). The ^{13}C CP/MAS NMR spectrum shows two resonances at 7.9 and 96.5 ppm that correspond to the methyl carbons and the cyclopentadienyl carbons respectively of the structure-directing agent (Figure 2b). Strong spinning side bands observed for the aromatic resonanaces may indicate that the ring carbons are held relatively rigidly inside the zeolite pores (it is not possible to extract or ion exchange the metal complex). The ^{1}H NMR spectrum for the as-made material (Figure 2c) shows an intense resonance at 1.5 ppm, assigned to the protons of the organic structure-directing agent. The ^{1}H NMR also shows a small resonance ~10 ppm probably due to defect sites of the form SiO$^-$···HOSi.[30] This is consistent with the fact that the cobalt complex in the pore has a net positive charge that, in the absence of tetrahedral 3+ framework atoms, i.e., Al or B, is balanced by a defect (siloxy group).[30] These results also show that the structure-directing agent is intact

(25) Rappe, A. K.; Casewit, C. J.; Colwell, K. S.; Goddard, W. A.; Skiff, W. M. *J. Am. Chem. Soc.* **1992**, *114*, 10024−10035.

(26) (a) Dessau, R. M.; Schmitt, K. D.; Kerr, G. T.; Woolery, G. L.; Alemany, L. B. *J. Catal.* **1987**, *104*, 484−489. (b) Boxhoorn, G., Kortbeek, A. G. T. G., Hays, G. R., Alma, N. C. M. *Zeolites* **1984**, *4*, 15−21.

(27) Woolery, G. L.; Alemany, L. B.; Dessau, R. M.; Chester, A. W. *Zeolites* **1986**, *6*, 14−16.

(28) Hunger, M.; Karger, J.; Pfeifer, H.; Caro, J.; Zibrowius, B.; Bulow, M.; Mostowicz, R. *J. Chem. Soc., Faraday Trans. I* **1987**, *83*, 3459.

(29) Engelhardt, G.; Michel, D. *High-Resolution Solid-State NMR of Silicates and Zeolites*; Wiley: New York, 1987.

(30) Koller, H.; Lobo, R. F.; Burkett, S. L.; Davis, M. E. *J. Phys. Chem.* **1995**, *99*, 12588−12596.

(31) Lobo, R. F.; Zones, S. I.; Davis, M. E. *J. Inclusion Phenom.* **1995**, *21*, 47−78.

Table 1. Adsorption Capacities for UTD-1 and Other Molecular Sieves

adsorbate	kinetic diameter (Å)[b]	adsorption capacity (mL g^{-1})				
		SSZ-24	L	Y	UTD-1[a]	VPI-5[b]
n-hexane	4.4	0.101	0.152	0.277	0.121 (0.106)	0.198
2,2-dimethyl butane	6.2	0.128	0.126	0.251	0.119 (0.091)	0.148[f]
cyclohexane	6.0	0.124	0.108	0.244	0.111 (0.079)	0.156
1,3,5-triisopropyl benzene	~8.5	0.008	0.109[c]	0.170[d]	0.111[e] (0.063)	0.117

[a] Numbers in parentheses are the adsorption capacities of UTD-1 samples after calcination but before treatment with aqueous HCl. [b] From refs 24 and 34. [c] Average of three independent measurements, after 3 h of adsorption time. [d] Zeolite Y adsorbs 1,3,5-triisopropylbenzene very slowly; this measurement was taken after 5 days of adsorption time at room temperature. [e] Average of two independent measurements. [f] Adsorption capacity for neopentane.

inside the zeolite pores and that no decomposition products are occluded in the pores during the crystallization process.

^{29}Si NMR spectra of the calcined and acid-treated samples (collected with a recycle delay of 100s) are deconvoluted into three peaks at −102.9 (3.5%), −111.45 (71%), and −113.2 (25.5%) (Figure 2d). The resonance at −102.9 ppm is consistent with the presence of a small amount of silanol groups remaining after the removal of the structure-directing agent. Also, ^{29}Si CP/MAS NMR data from the calcined sample (not shown) show an enhancement of a resonance at −103 ppm in agreement with the premise that this resonance is due to a silanol group. The relative ratios of the two Q^4 resonances is almost 3 to 1 (various simulations result in relative ratios of 2.8 to 3.2). Given the site populations from the structure solution (see below) [Si1(8), Si2(8), Si3(16), Si4(16), Si5(16)] this relative intensity corresponds to a ratio of 48 to 16. Furthermore, when shorter recycle delay times are used, the relative intensity of these two peaks approaches 4, i.e., with shorter delay times the relative intensity of the resonance at −113.2 ppm diminishes. It is possible that a fraction of T atoms contributing to the peak at −113.2 ppm (the less intense resonance), have a longer T_1 relaxation time and it is only with longer recycle delays that this resonance can reach its maximum signal intensity. The following assignment is consistent with the structural model of UTD-1: Si1, Si3, Si4, and Si5 are all readily accessible by oxygen molecules inside the channel and can relax with short delay times. Si2, however, has no direct access to the channel system, hence its longer relaxation time. Thus, the assignment of the two observed bands is that Si3, Si4, and Si5 (total population 48) comprise the resonance at −111.4 ppm and Si1 and Si2 (total population = 16) comprise the peak a −113.2 ppm.

Adsorption Studies. Adsorption capacity measurements of organic molecules in UTD-1 are in agreement with the reported structure of UTD-1. Table 1 shows the adsorption capacity of several large-pore zeolites and UTD-1. The adsorption capacity of UTD-1 is very similar to the adsorption capacity of SSZ-24 (AFI), a one-dimensional large pore molecular sieve (7.3 Å in diameter),[32,33] and it is clearly smaller than the adsorption capacity of a three-dimensional large pore zeolite (FAU) and the one-dimensional 18MR VPI-5 (12.1 Å in diameter).[13] The adsorption capacity of UTD-1, for 2,2-dimethylbutane and cyclohexane shows that UTD-1 is at least a large-pore material. Comparison of the adsorption capacity for 1,3,5-triisopropylbenzene of zeolite L, zeolite Y, UTD-1 and VPI-5 shows that the molecule of 1,3,5-triisopropylbenzene (with a kinetic diameter of ~8.5 Å) is close to the maximum molecular size which can pass the 14-rings at this temperature.[34] The adsorption capacity for 1,3,5-triisopropylbenzene of UTD-1 is in agreement with the one-dimensional 14MR pore system reported by Freyhardt et al.[12]

There is a systematic difference in the adsorption capacities of samples analyzed before or after acid treatment. The adsorption capacities of calcined Co-containing UTD-1 samples are lower than the capacities of samples treated with aqueous HCl, especially for the larger adsorbent molecules. Apparently, the channels of Co-UTD-1 are partially blocked by occluded cobalt oxide left inside the sample after calcination. Bright-field TEM of the cobalt-containing samples (see Supporting Information) shows cobalt oxide particles both on the crystal surface and occluded within the 14MR pores.[35] It is also noted that 1,3,5-triisopropylbenzene adsorbs in Co-containing UTD-1 as rapidly as in Co-free UTD-1. Thus, either the small cobalt particles occluded in the pores act as a barrier to stop the diffusion of this large organic molecule beyond certain section of the pore, and/or only a fraction of the pores contains occluded cobalt. The cobalt particles do not change significantly the adsorption of smaller molecules. The rate of adsorption of the smaller and flexible *n*-hexane adsorbate is slowed only slightly, and the nitrogen adsorption data (not shown) also show approximately similar diffusion rates and total uptake in Co-containing UTD-1 as in Co-free samples. The adsorption data suggest as a whole, that indeed Co oxide is occluded in the pores just after calcination and that the effect of the cobalt must be taken into account for the evaluation of diffusion/catalytic properties. Fortunately, the cobalt oxide is completely removed by the acid treatment (verified by chemical analysis), yielding complete access to the pores of the material.

The geometrically calculated void volume for the model (see below) is ~990 Å^3 per unit cell (0.15 mL g^{-1}) which is in agreement with the adsorption capacities reported in Table 1. The adsorption capacity data are somewhat smaller than the values expected from the TGA of the as-synthesized UTD-1. TGA shows a weight-loss event of ~13.1% between 200 and 800 °C. This event has been assigned to the pyrolysis and combustion of the cobalt complex. Note that an exact comparison of the TGA weight loss to the adsorption data is not possible due to unknown amounts of cobalt oxide in the sample after heating to 800 °C.

Characterization of UTD-1 by Diffraction and TEM Methods

X-ray Diffraction Data. The X-ray powder diffraction pattern of UTD-1 (see below) can be indexed using an orthorhombic unit cell with lattice constants of approximately a = 18.98 Å, b = 8.41 Å, and c = 23.04 Å. The d spacings and indexing of the experimental pattern are presented in Table 2. The systematic absences are in agreement with a body centered unit cell ($h + k + l = 2n$), and $k = 2n$ for all reflections

(32) Bialek, R.; Meier, W. M.; Davis, M. E.; Annen, M. J. *Zeolites* **1991**, *11*, 438−442.
(33) Richardson, J. W.; Smith, J. V.; Han, S. X. *J. Chem. Soc., Faraday Trans.* **1990**, *86*, 2341.
(34) Davis, M. E.; Montes, C.; Hathaway, P. E.; Arhancet, J. P.; Hasha, D. L.; Garces, G. *J. Am. Chem. Soc.* **1989**, *111*, 3919.
(35) Balkus, K. J.; Biscotto, M.; Gabrielov, A. G. *Stud. Surf. Sci. Catal.* **1997**, *105*, 415−423.

Table 2. *d* Spacings and Indexing for calcined UTD-1[a]

h	*k*	*l*	*d* (Å)	I/I_0
1	0	1	14.66	100
0	0	2	11.53	38
2	0	0	9.50	4.9
1	0	3	7.13	0.3
3	0	1	6.12	4.4
0	0	4	5.76	0.3
2	0	4	4.93	1.9
3	0	3	4.90	3.5
1	0	5	4.49	5.8
4	0	2	4.40	1.6
0	2	0	4.21	17.9
1	2	1	4.05	3.6
(0	1	5)	4.05	3.6
0	2	2	3.97	2.6
0	0	6	3.85	1.9
5	0	1	3.74	0.9
4	0	4	3.67	3.7
2	0	6	3.56	3.4
3	2	1	3.46	0.5
5	0	3	3.40	2.0
3	2	3	3.19	0.9
6	0	0	3.16	2.6
1	2	5	3.07	1.2
6	0	2	3.05	1.0
4	2	2	3.03	0.5
4	0	6	2.98	1.5
0	2	6	2.84	0.3
4	2	4	2.76	1.4
(6	1	3)	2.76	1.4
2	2	6	2.72	0.7
7	0	1	2.69	0.3
5	2	3	2.65	0.7
7	0	3	2.56	0.5
6	2	0	2.53	1.0
6	2	2	2.47	0.5
4	2	6	2.43	0.9

[a] On the basis of the X-ray powder diffraction data only, the reflections in parentheses cannot be unambigously excluded from the XRD pattern because of overlap with the previous reflection. However, the ED data (see text) clearly indicates that these two reflections are actually *not* present in the pattern.

except, perhaps, for the two entries indicated in parentheses in Table 2. The presence or absence of these two reflections in the XRD pattern cannot be unambiguously confirmed because of overlap with other reflections. These reflections are, nonetheless, excluded from the pattern on the basis of ED data (see below). The absence of all reflections with $k = 2n + 1$ suggests the presence of stacking faults and/or disorder along the *b* axis. The presence of this type of stacking faults/disorder is also in agreement with electron diffraction data (*vide infra*). As a consequence of the disorder, the systematic absences obtained from the analyses of the XRD data cannot be used to discriminate between different space groups.

Electron Diffraction and Transmission Electron Microscopy. The transmission electron micrographs shown in Figure 3 reveal that the UTD-1 particles are aggregates of faceted, elongated platelets about 5 μm long and 0.1 μm wide. In the bright field image (Figure 3b) fringes corresponding to the (101) planes are resolved running down the long axis of the platelets; i.e., the channels with the 14 T-atom pore opening are running down the long axis of the crystals.

Characteristic electron diffraction patterns are given in Figure 4. Figure 4a is a diffraction pattern with the electron beam perpendicular to the basal plane of the crystals (see Figure 2b), i.e., the [101] zone axis. This selected-area diffraction pattern shows alternating rows of sharp and streaking spots. The sharp spots occur at rows with $k = 2n$, and the streaked spots occur at rows with $k = 2n \pm 1$ ($n = 0, \pm1, \pm2$, etc.). Recall that XRD data show the absence of such reflections. Streaking is along a direction perpendicular to the b^* reciprocal axis. This observation suggests also disorder and/or faulting along the *b* axis, i.e., along the long axis of the crystals that coincides with the direction of the 14 T-atom pores. The presence of sharp spots every second column suggests translations of $\pm^1/_2 b$ axis. The intensity of streaking decreases from the [100] (maximum streaking) to the [101] (some streaking) to [001] (no streaking) zone axes. Figure 4b and 4c are diffraction patterns from the [001] zone axis and tilted by few degrees from the [001] axis respectively. Only sharp spots are observed in Figure 4b with $h+k = 2n$ and $k = 2n$. However, tilting around the *b* axis leads to diffraction patterns as the one shown in Figure 4c where spots with $h + k = 2n + 1$ as well as $k = 2n + 1$ appear. The appearance of these additional spots can be understood by considering the reciprocal space which is streaked along [001] due to the faulting/disorder within the (002) planes. Depending on the tilt, when close to the [001] zone axes, the Ewald sphere can intercept a streak rather than a sharp Bragg reflection. For tilts up to $\pm20°$, the pattern can maintain the appearance of high symmetry, where all or some of the forbidden reflections are observed. However, accurate orientation leads to the pattern shown in Figure 4b, where the spots are considered to be due to sharp Bragg reflections. These results are in agreement with the premise that faulting is within the (002) planes. Moreover, such disorder and/or faulting will not affect the 14-member ring channels. This is shown in Figure 3c, which shows no distortions in the view down the *b* axis. An electron diffraction pattern with the electron beam along the *b* axis ([010] zone axis) is shown in Figure 4d. The (*h*0*l*) reflections are all sharp and systematic absences are observed for $h + l = 2n + 1$, suggesting a centered unit cell in agreement with the XRD data that show $h + k + l = 2n$. The intensities of the (*hkl*) spots with $k = 2n + 1$ (along the streaked columns) in Figure 4a are much less pronounced than the (*hkl*) spots with $k = 2n$. Since (*hkl*) spots with $k = 2n + 1$ are forbidden in body-centered cells and allowed in face-centered cells, their presence with small intensities suggests an intergrowth of body and face-centered unit cells.

High-Resolution Electron Microscopy. HREM was carried out along the *b*-axis direction which gives the diffraction pattern with the sharp spots shown in Figure 4d. The HREM image from a microtomed section of UTD-1 is shown Figure 5a (the original image) while Figure 5b is the FFT-enhanced image. The resolution of the original image, which was recorded at near optimum defocus, is about 2 Å as evidenced by optical diffraction. In addition to the 14-ring, the 5- and 6-rings are clearly resolved having substantially different intensities. It is known that for thin zeolite samples and under the Scherzer or optimum focusing condition, the 2D, 3-connected net of the structure can be derived from electron micrographs.[36−38] It should be noted that the 4-rings do not appear as white dots, as confirmed by the simulation shown in Figure 5c, but their presence is suggested from the spacing of the net in the corresponding positions. The 2D, 3-connected net shown in Figure 5d can be devised from the HREM image. Attempts to acquire similar information in directions perpendicular to the channel length ([100] and [101] zone axes) did not result in images that can be interpreted in terms of projected potential.

Structure Solution and Disorder in UTD-1. The structure of UTD-1 was solved by an iterative process of model building, distance least-square refinement, and comparison of simulated

(36) Pan, M. *Micron* **1996**, *27*, 219−238.
(37) Terasaki, O.; Ohsuna, T. *Catal. Today* **1995**, *23*, 201−218.
(38) Terasaki, O.; Ohsuna, T.; Sakuma, H.; Watanabe, D.; Nakagawa, Y.; Medrud, R. *Chem. Mater.* **1996**, *8*, 463−468.

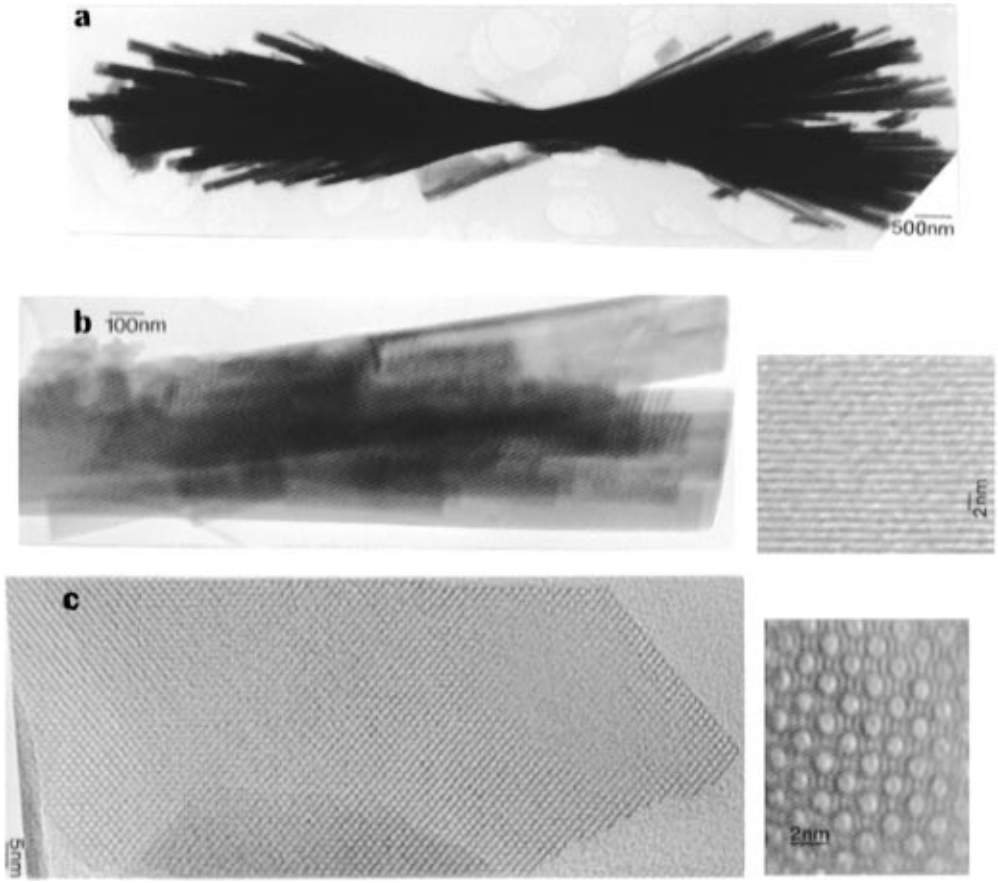

Figure 3. Transmission electron micrographs of UTD-1: Parts a and b are views perpendicular to the 14-MR channels; (c) is a veiw parallel to the 14-MR channels.

and experimental XRD patterns. The unit cell parameters of UTD-1 (a = 18.98 Å, b = 8.41 Å, and c = 23.04 Å) suggest that this material is related to ZSM-48 (orthorhombic, a = 14.24 Å, b = 20.14 Å, and c = 8.40 Å)[39] and SSZ-24 (AFI) (hexagonal, $a = b$ = 13.65 Å and c = 8.35 Å).[32,33] These two high-silica zeolites are one-dimensional pore materials formed by sheets of atoms in an Up−Down combination (denoted ○●). On the basis of the results from HREM, a framework with the correct magnitude for a and c can be formed from the σ expansion of a ferrierite sheet, forming a new "UTD-1" sheet as indicated in Scheme 2.

If UTD-1 is either body (*I*) or face-centered (*B*), as indicated by the diffraction data, then there are five independent tetrahedral atoms in the asymmetric unit. In principle these can be combined to form 60 (15 for each space group *Imma*, *Immm*, *Bmmm*, and *Bmmb*) related structures. The search has been restricted initially to structures in which the connectivity of the T atoms that forms the channel surface is formed by a cylindrical 6-ring net (as it is also reported for ZSM-48 and SSZ-24 and SSZ-31).[32,40] This means that there must be a strict alternation of UDUD T atoms (denoted ○●○●..., in Figure 6) throughout the 14MR of the zeolite. In addition, since high-silica zeolites show only a relatively small number of 4-rings in the structure, the candidate topologies with small number of 4-rings are preferred over those with larger number of 4-rings.[41] Note that since all 60 structures have the same framework density, pore diameter and projected potential along the [010] axis, adsorption capacities, unit cell lattice parameters, and HRTEM micrographs cannot be used to differentiate between the frameworks as to which is a better model for UTD-1. To do this, comparison of experimental and simulated of X-ray powder diffraction patterns is necessary.

One possible framework topology is shown in Figure 6a. This topology belongs to space group *Imma* (reported initially in ref 9 and denoted from now on as polymorph A), has a cylindrical 6-ring net pore, and contains the so called UDUD (○●○●) narsarsukite chains along the pore direction (see Figure 7). These chains are also present in the all-silica SSZ-24 (AFI).[32] The simulated XRD pattern of the distance least-squares refined structure of this model shows many similarities to the experimental pattern of UTD-1, but also several discrepancies. The discrepancies are all associated with *hkl* reflections with index $k = 2n + 1$, that are observed in the simulated XRD pattern but not in the experimental pattern. Faulting/disorder along $\pm^1/_2 b$ of the material is one possible explanation for the absence of $k = 2n + 1$ reflections. Since electron diffraction data show conclusively that faulting occurs along the (002) planes and that the faulting involves translations of $\pm^1/_2 b$, the effect of faulting is investigated in detail.

The effect on the XRD pattern of this type of faulting was investigated using simulations of intergrowth structures with the program DiFFAX.[42] Periodic faulting of $\pm^1/_2 b$ within the 002 planes of polymorph A (*Imma*) forms a new framework with the *Bmmm* space group (no. 65, nonstandard setting, denoted polymorph B). Note that in Figure 6a, a translation of $\pm^1/_2 b$ is equivalent to changing an up T atom for a down T

(39) Schlenker, J. L.; Rohrbaugh, W. J.; Chu, P.; Valyocsik, E. W.; Kokotailo, G. T. *Zeolites* **1985**, *5*, 355−358.

(40) Higgins, J. B. High-Silica Zeolites. In *Silica: Physical Behavior, Geochemistry and Materials Applications*; Heaney, P. J., Prewitt, C. T., Gibbs, G. V., Eds.; Mineralogical Society of America: Washington, 1994.

(41) Lobo, R. F.; Tsapatsis, M.; Freyhardt, C. C.; Chan, I. Y.; Chen, C. Y.; Zones, S. I.; Davis, M. E. *J. Am. Chem. Soc.* **1997**, *119*, 3732−3744.

(42) Treacy, M. M. J.; Newsam, J. M.; Deem, M. W. *Proc. R. Soc. London A* **1991**, *433*, 499−520.

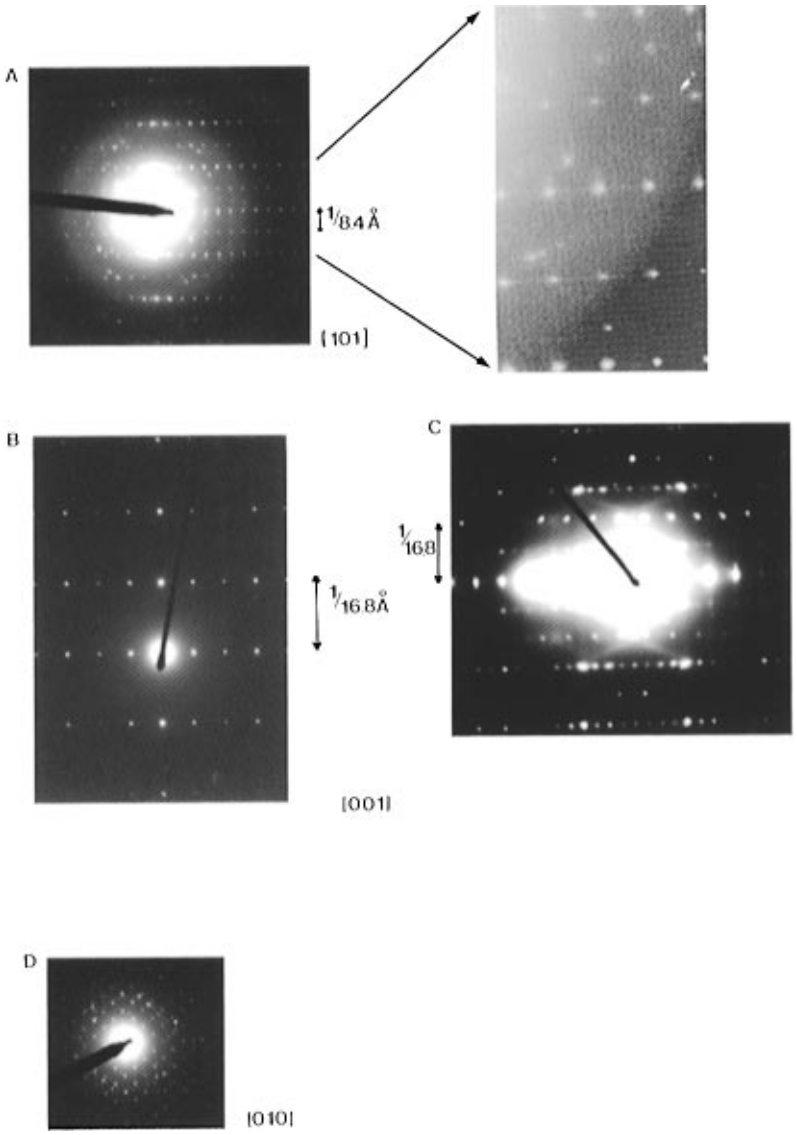

Figure 4. Electron diffraction patterns of UTD-1. Part a is a diffraction pattern with [101] zone axis (the magnified inset shows the streaking every other row), and d is a diffraction pattern with [010] zone axis. Parts b and c are diffraction patterns with [001] zone axis and tilted by 10° from the [001] direction, respectively.

atom and vise versa; and that this faulting breaks the alternating UDUD sequence allowing 4MRs and 8MRs in the inner surface of the pores.[12] Effectively, this type of faulting maintains the connectivity within the $5^2 4^1$ layers described in Scheme 1 and just changes the connectivity between the layers. (See ref 12 for more details about polymorphs A and B.)

The simulations of the XRD patterns of intergrowths of polymorphs A and B are presented in Figure 8a. Here it is assumed that the faulting is completely random and that the disorder can be described only by one parameter *p*. (For more details on the use of DIFFaX see refs. 41 and 43 and the manual of DIFFaX). This parameter is the probability that after any layer the stacking vector relating two consecutive layers is given by $\mathbf{R} = {}^1/_2a + {}^1/_2c$, i.e., face centering and not by $\mathbf{R} = {}^1/_2a + {}^1/_2b + {}^1/_2c$, body centering, as would be for polymorph A. A stacking probability $p = 0\%$ forms the polymorph A and a stacking probability of 100% forms the polymorph B. A close match between the calculated and experimental XRD patterns is obtained for a material with a fault probability of approximately 20%. This is the proposed structure solution provided for UTD-1 in ref 12.

A second topology with a cylindrical 6-ring net pore is shown in Figure 6c. This framework belongs to the *Bmmb* space group (no. 63, nonstandard setting, denoted polymorph C) and contains UUDD chains (double crankshaft chains, see Figure 7). The atomic coordinates of the distance least-square (DLS-76)[44] refined structure are presented in Table 3. As it was the case with the previous model, the XRD pattern of this polymorph also shows many similarities to the experimental XRD of UTD-1. Periodic faulting of $\pm{}^1/_2b$ within the 002 planes of polymorph C (*Bmmb*) forms a new framework with the *Immm* space group (no. 71, see Figure 6d and Table 4) denoted polymorph D. This framework also contains 4MRs and 8MRs in the inner surface of the pores as polymorph B. Simulations of the XRD patterns of intergrowths of these two polymorphs are presented in Figure 8b. As before, it is assumed that the intergrowths are completely random and that the disorder is described by only one parameter *p*. The stacking vector to form a layer of polymorph C is $\mathbf{R} = {}^1/_2a + {}^1/_2c$, face centering, and the stacking vector to form a layer of polymorph D is $\mathbf{R} = {}^1/_2a + {}^1/_2b + {}^1/_2c$, body centering. A very good match between the calculated and experimental

(43) Treacy, M. M. J.; Vaughan, D. E. W.; Strohmaier, K. G.; Newsam, J. M. *Proc. R. Soc. London A* **1996**, *452*, 813−840.

(44) Baerlocher, C.; Hepp, A.; Meier, W. M. DLS-76: A Fortran Program for the Simulation of Crystal Structures by Geometric Refinement; Institut fuer Kristallographie, ETH: Zurich, 1977.

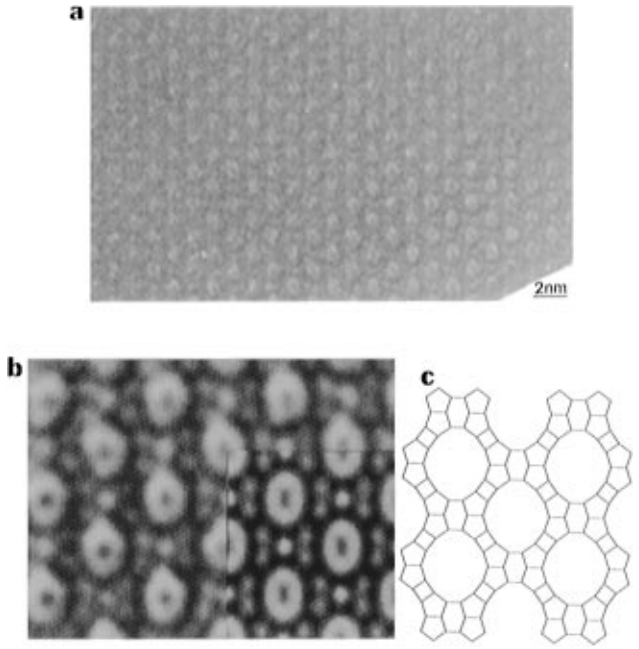

Figure 5. High-resolution electron-micrograph view down the 14-MR channels. Part a is the image as recorded while b is the processed image using FFT filtering. The simulated projection is shown in the inset, and the derived 2-D net in c.

Scheme 2

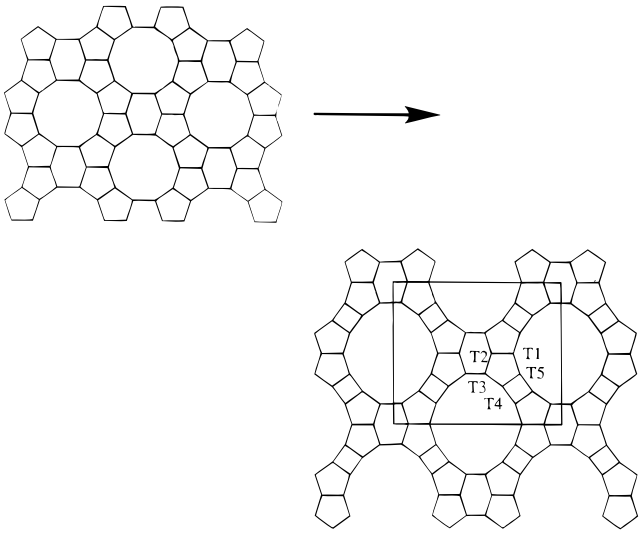

XRD patterns is also obtained for a material with a fault probability of ∼50%.

A third alternative intergrowth structure with cylindrical 6-ring net pores can also be obtained from combining the up/down 5^24^1 layers of polymorph A, and the up/down layers 5^24^1 layers of polymorph C. The disorder in this material could be also characterized as due to the presence of the narsarsukite chains and the double-crankshaft chains in different layers. The main difference between this intergrowth and the previous two intergrowths is the pores (see Supporting Information). In this case, the pores are formed only of 6-ring cylindrical nets; no 4MRs or 8MRs are present in the inner surface of the channels. A good agreement between calculated and experimental XRD patterns is observed in these simulations for fault probabilities ∼50% (see Supporting Information).

There are other alternative topologies that could be proposed. However, we have been unable to find any other topology in which there is either a large number of adjacent 4MR, or there are secondary building units with no historical precedent in any known zeolite silicate structure. These structures are considered unlikely and have not been investigated in detail.

The good agreement between the XRD patterns of the three proposed intergrowth structures (Figure 9) and the experimental pattern establish, without ambiguity, that the framework structure of UTD-1 consists of the "expanded ferrierite" or UTD-1 sheets (parallel to the *ac* plane). The tetrahedral atoms in each layer point down or up, and the oxygens are located in the mirror planes between each UTD-1 sheet. Of the three intergrowths presented in Figure 9, the intergrowth of the structures with *Bmmb* and *Immm* space groups (polymorphs C and D, see Figure 9a) shows the closest agreement to the experimental pattern. These two models contain the double-crankshaft chains (UUDD) and are different from the original proposed intergrowth model for UTD-1 that contains the narsarsukite chains (UDUD). There is still small disagreement at $2\theta > 25$, but this may be due to small errors in the positions of oxygen and silicon atoms within each layer (only optimized here using DLS-76) and/or an indication that other intergrowths and/or other up/down sequences may be also present in the material in smaller amounts.

In summary, using electron microscopy, solid-state NMR spectroscopy, adsorption studies, and simulation of X-ray powder diffraction patterns, we have shown that UTD-1 is a high-silica zeolite with a one-dimensional 14MR pore architecture. The structure is heavily faulted with faults parallel to the (002) planes. The fault planes do not block the pore apertures. We have also identified a structural model for the framework topology of the UTD-1. This model is an intergrowth of what we denote as polymorphs C and D and contains the so-called double-crankshaft chains running down the pore axis. Simulation of a random intergrowth of equal amounts of these polymorphs shows a very good agreement between the simulated and experimental X-ray powder diffraction patterns.

Finally, we want to point out the close structural relationships between UTD-1 and ZSM-48. In both materials, the main structural unit within the channel walls consists of a double layer containing one 6MR surrounded by four 5 MRs (5^46^1). The up and down sequence of T atoms in polymorph A of UTD-1 is the same as the one proposed by Schlenker et al.[39] for the UUDD-*Cmcm* polymorph of ZSM-48. Moreover, the up and down sequence in polymorph C of UTD-1 is the same as the UDUD-*Imma* of ZSM-48. Both UTD-1 and ZSM-48 show disorder in the structure due to the presence of different UD sequences in the structure.

Thermal and Hydrothermal Stability of UTD-1. The thermal and hydrothermal stability of UTD-1 is investigated using *in situ* X-ray powder diffraction of samples treated at different temperatures. A dry nitrogen atmosphere is used for thermal stability studies, and a water/nitrogen atmosphere is used for hydrothermal stability. Figure 10 shows the XRD patterns of UTD-1 at selected temperatures in the presence of water vapor in the nitrogen atmosphere. As it can be observed, little if any, loss of crystallinity is detected at temperatures up to 1000 °C. After the high-temperature treatment and decrease of the sample temperature back to 25 °C, the XRD pattern is almost indistinguishable from the original XRD pattern. Similar results are observed for the samples investigated under a dry nitrogen atmosphere (not shown). These results show conclusively that UTD-1, despite the large pore apertures, has a thermal/hydrothermal stability comparable to medium- and large-pore high-silica zeolites.

Catalytic Activity of Aluminum-Containing UTD-1. ^{27}Al MAS NMR spectroscopy of Al-UTD-1 shows the presence of two peaks at 55 and ∼0 ppm. These two peaks indicate the

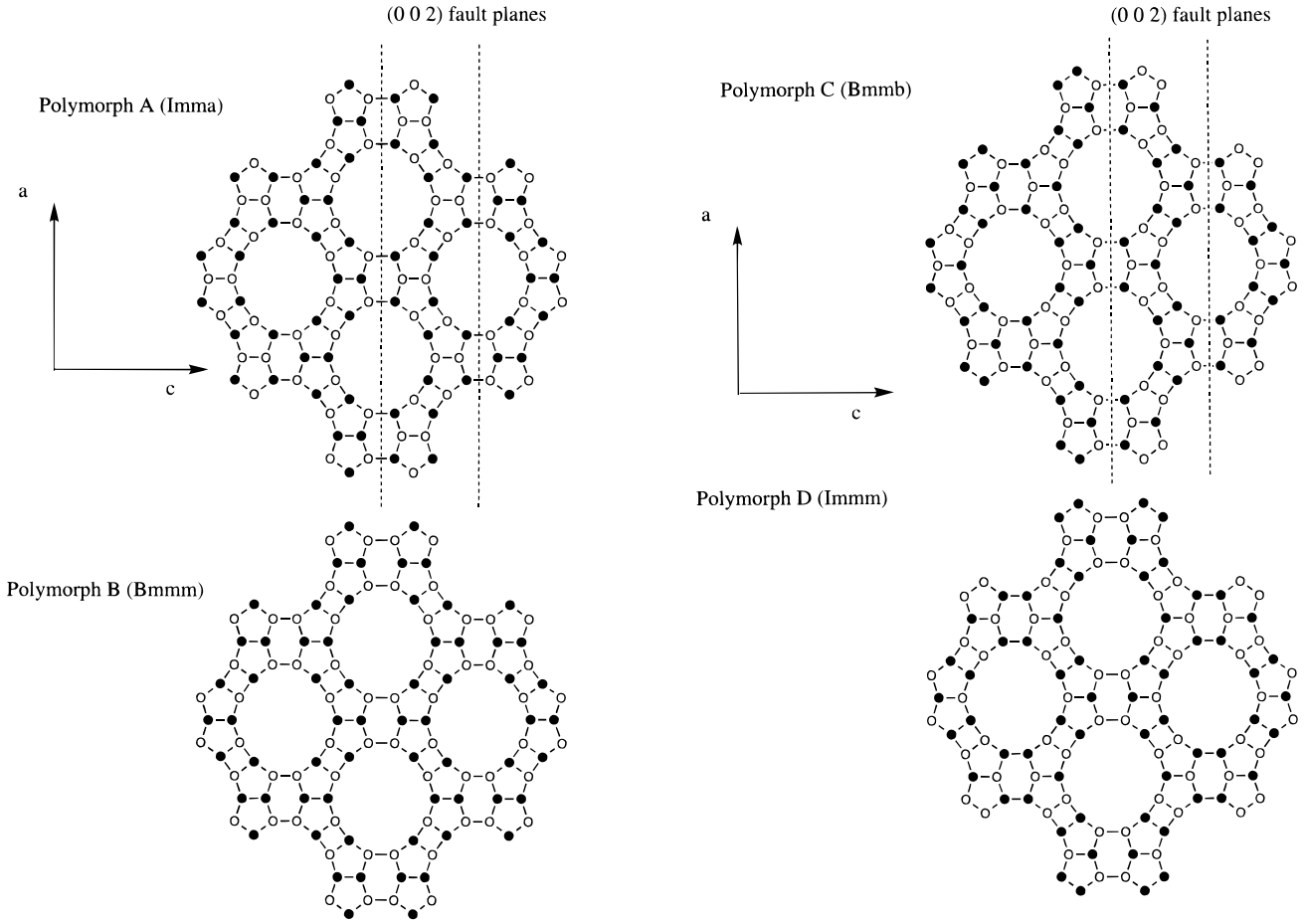

Figure 6. Up and down (○●) configuration of the tetrahedral atoms in different framework topologies of UTD-1: (a) polymorph A, top-left; (b) polymorph B; (c) polymorph C, top-right; and (d) polymorph D. The dotted lines in a indicate the "layers" used in the simulations of XRD patterns of faulted materials using DIFFaX.

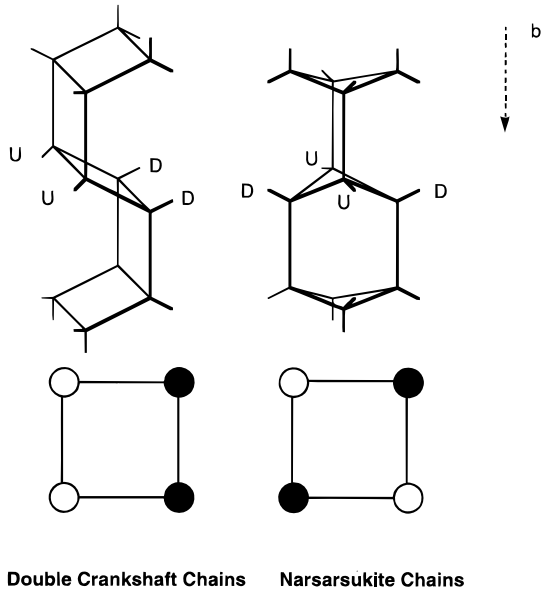

Figure 7. Narsarsukite (UDUD) and double-crankshaft chains (UUDD) of tetrahedral atoms connecting successive layers of T-atoms in polymorphs A and B (narsarsukite) and polymorphs C and D (double-crankshaft).

presence of tetrahedral aluminum (at 55 ppm) and octahedral aluminum (∼0 ppm) in the sample, after the treatment with an aqueous aluminum nitrate solution. On the basis of the relative areas of these two peaks, it is estimated that the sample contains tetrahedral and octahedral aluminum in a ratio of approximately 85:15. Chemical analysis also reveals a SiO_2/Al_2O_3 ratio of almost 70.

We attempted to characterize the samples of Al-UTD-1 using the isopropylamine desorption method described by Gorte et al.[45] to quantify precisely the number density of acid sites in the sample. We have found that for our experimental conditions, if the samples contain appreciable amounts of octahedral aluminum, i.e., Lewis acid sites as in UTD-1, the propene formed as a result of the amine decomposition oligomerizes. Thus, the desorption results cannot be used to accurately determine the acid site density in Al-UTD-1.[46]

Several aspects of the catalytic activity and selectivity of zeolite Al-UTD-1 resemble the properties of large-pore zeolites like zeolite L and mordenite. Recall that zeolite L and mordenite have a corrugated one-dimensional pore system, and these corrugations effectively expand the cross section diameters of the pores. For example, the conversion of *m*-xylene using Al-UTD-1 as the catalyst decreased monotonically from 22% after 120 min of reaction on stream, to ∼5% after 1000 min (17 h) of reaction time. The relative distribution of trimethylbenzenes was 0.71:0.21:0.08 for the 1,3,5-, 1,2,4-, and 1,2,3-trimethylbenzene isomers, respectively. This distribution is similar to the distribution observed for other large-pore high-silica zeolites,[47−49,8] and it is near the distribution expected from

(45) Farneth, W. E.; Gorte, R. J. *Chem. Rev.* **1995**, *95*, 615−635.

(46) Unlike Gorte et al. (see ref 45) we carry out the desorption of the amine from the zeolite in flowing He gas at 1 bar. Gorte et al. carry out their desorption experiments in vacuum and this may be the reason for the polymerization of the propene in the zeolite pores in our experiment.

(47) Perez-Pariente, J.; Sastre, E.; Fornes, V.; Martens, J. A.; Jacobs, P. A.; Corma, A. *Appl. Catal.* **1991**, *69*, 125−137.

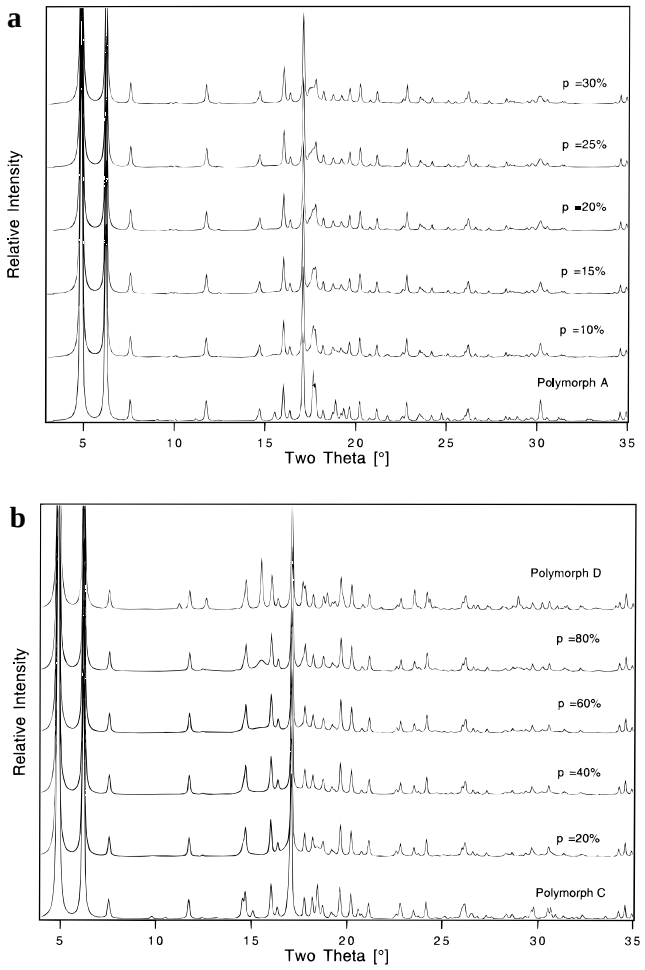

Figure 8. Effect of faulting on the X-ray powder diffraction patterns of intergrowths of polymorphs A and B (a), and of polymorphs C and D (b). The instrumental peak broadening was simulated using the pseudo-Voigt function with $u = 0.2$, $v = -0.18$, $w = 0.05$, and $\gamma = 0.6$ ($\lambda = 1.2513$ Å).

Table 3. Fractional Atomic Coordinates for Polymorph C, *Bmmb* (No. 63, Nonstandard Setting) UTD-1 [$Si_{64}O_{128}$]

atom	multiplicity, Wyckoff letter	*x*	*y*	*z*
Si1	8f	0.5	0.4356	0.3812
Si2	8f	0.5	0.5658	0.2551
Si3	16h	0.3579	0.4368	0.2284
Si4	16h	0.2682	0.4374	0.3348
Si5	16h	0.3568	0.5619	0.4351
O11	4c	0.5	0.25	0.3942
O12	8f	0.5	0.4640	0.3131
O15	16h	0.4314	0.5144	0.4087
O22	4c	0.5	0.75	0.2707
O23	16h	0.4313	0.5243	0.2184
O33	8g	0.3703	0.25	0.2307
O34	16h	0.3242	0.4947	0.2878
O43	16h	0.1944	0.5217	0.3231
O44	8g	0.2588	0.25	0.3305
O45	16h	0.2957	0.4832	0.3976
O55	8g	0.3484	0.75	0.4341
O55a	8e	0.3517	0.5	0.5

thermodynamic equilibrium. In addition, the rate of isomerization/disproportionation was lower than 1.8 at all times, similar to the rates of isomerization of other large pore zeolites (mordenite, L, and Y). Interestingly, the para/ortho ratio of the product was 0.8 or lower during the entire reaction period (17 h). Further details of acidity and catalytic properties of UTD-1 will be reported at a later date.[50]

(48) Martens, J. A.; Perez-Pariente, J.; Sastre, E.; Corma, A.; Jacobs, P. A. *Appl. Catal.* **1988**, *45*, 85−101.
(49) Weitkamp, J.; Ernst, S. *Catal. Today* **1994**, *19*, 107−150.

Table 4. Fractional Atomic Coordinates for Polymorph D (Space Group *Immm* No. 71) of UTD-1 [$Si_{64}O_{128}$]

atom	multiplicity, Wyckoff letter	*x*	*y*	*z*
Si1	8l	0.5	0.6856	0.3812
Si2	8l	0.5	0.8158	0.2551
Si3	16o	0.3579	0.6868	0.2284
Si4	16o	0.2682	0.6874	0.3348
Si5	16o	0.3568	0.8119	0.4351
O11	4i	0.5	0.5	0.3942
O12	8l	0.5	0.7140	0.3131
O15	16o	0.4314	0.7644	0.4087
O22	4j	0.5	0	0.2707
O23	16o	0.4313	0.7743	0.2184
O33	8m	0.3703	0.5	0.2307
O34	16o	0.3242	0.7447	0.2878
O43	16o	0.1944	0.7717	0.3231
O44	8m	0.2588	0.5	0.3305
O45	16o	0.2957	0.7332	0.3976
O55	8m	0.3484	0	0.4341
O55a	8n	0.3517	0.75	0.5

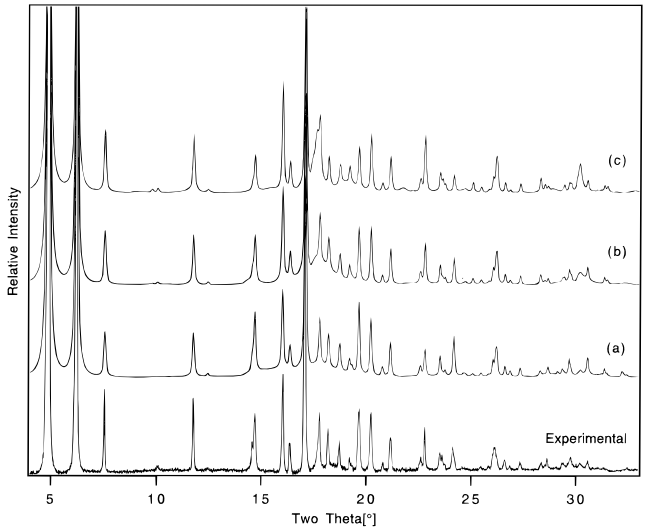

Figure 9. Comparison of the simulated X-ray powder diffraction patterns of the three proposed intergrowth structures with the experimental XRD patterns ($\lambda = 1.2514$ Å): (a) intergrowth of polymorphs C and D with $p = 50\%$; (b) intergrowth of polymorphs A and C, $p = 50\%$; and (c) intergrowth of polymorphs A and B, $p = 20\%$. The instrumental peak broadening was simulated using the pseudo-Voigt function with $u = 0.1$, $v = -0.036$, $w = 0.009$, and $\gamma = 0.6$.

Packing Arrangement of $[(Cp^*)_2\ Co]^+$ Occluded in the Micropores. To address the question of the orientation of the structure-directing agent inside the pores of UTD-1, we have used energy-minimization calculations. We have followed the procedures reported by Shen and Bell,[51] and Lewis et al.[52] to carry out the minimizations: (i) the zeolite framework is fixed during the minimization and only the structure-directing molecule (1 per unit cell) is allowed to move, and in a second calculation (ii) the zeolite framework and the organometallic molecule are allowed to relax. Moreover, no charges are assigned to the framework and the molecule for the calculations.[52]

Two orientations of the organometallic molecule where investigated in detail: (i) the molecule has its 5-fold axis of symmetry approximately collinear with the *a* axis of the crystal

(50) Khodabandeh, S.; Davis, M. E. Manuscript in preparation, 1997.
(51) Shen, V.; Bell, A. T. *Microporous Mater.* **1996**, *7*, 187−199.
(52) Lewis, D. W.; Freeman, C. M.; Catlow, C. R. A. *J. Phys. Chem.* **1995**, *99*, 11194−11202.

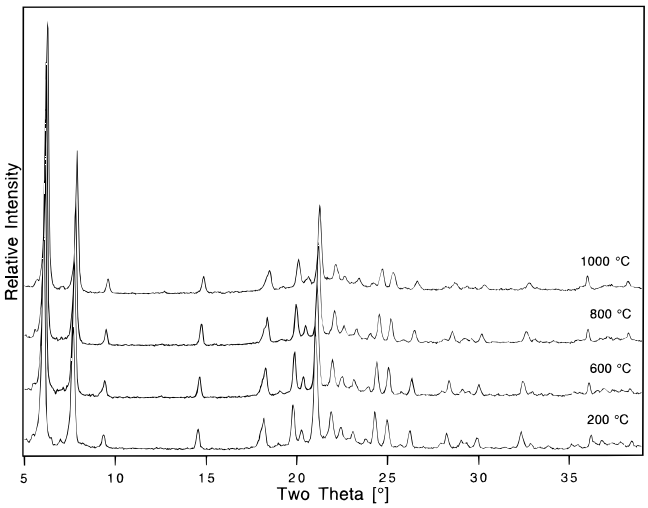

Figure 10. Variable-temperature X-ray powder diffraction patterns of UTD-1 in a water vapor/nitrogen atmosphere (λ = 1.5428 Å).

Table 5. Results from Energy Minimization Calculations of $[(Cp^*)_2Co]^+$ inside the Pores of UTD-1

		total energies (kcal/mol)			
		framework (fixed) + $[(Cp^*)_2Co]^+$		framework (flexible) + $[(Cp^*)_2Co]^+$	
	framework	5-fold axis along *a*	5-fold axis along *b*	5-fold axis along *a*	5-fold axis along *b*
polymorph C	−301	+1334	+1337	+1035	+1033
polymorph D	−298	+1332	+1340	+1034	+1039

[a] All the energies correspond to the total energy of the organometallic complex + all-silica framework as obtained from the energy minimization. [b] The energy of $[(Cp^*)_2Co]^+$ calculated in free space is +1399 kcal/mol.

system; and (ii) the 5-fold axis of symmetry is collinear with the *b* axis of the crystal. A summary of the results is presented in Table 5. As it can be observed, the differences in total energy between the two conformations are very small. These results are similar for both polymorphs C and D. The only notable difference between the energy minima is observed for the case in which the 5-fold axis of the molecule is collinear with *a*. In polymorph C, this axis is almost parallel to *a*, and in contrast, the 5-fold axis is slanted ∼15° from *a* in polymorph D. Qualitatively, the molecule in the latter case reduces its total energy by aligning the two opposite methyl groups along the 8-ring windows formed on the (002) planes as discussed above. Thus, on the basis of these calculations it is not possible to distinguish between the two conformations investigated. However, $Cp^*_2Co^+$ is not spherical, and intuitively we expect the complex to orient itself. A more comprehensive investigation will be necessary to address this issue.

Summary

Numerous characterizations of the zeolite UTD-1 confirm that it contains a one-dimensional, extra-large 14-ring pore system. TEM and ED show that UTD-1 is faulted along the (002) planes. It is determined—using simulation of XRD patterns of faulted structures—that among several possible faulted frameworks investigated, the XRD pattern of a framework containing double-crankshaft chains shows the best agreement with the experimental pattern. It is concluded that UTD-1 is an intergrowth of what we denote as polymorphs C and D. Thermal/hydrothermal stability studies show that UTD-1 has similar stability to medium- and large-pore high-silica zeolites. The ratio of isomerization to disproportionation, and the distribution of trimethylbenzene isomers in the *m*-xylene isomerization test reaction using UTD-1 are similar to those from other large-pore zeolites (zeolites Y or L). However, UTD-1 reveals a *p*-/*o*-xylene ratio of products below one (unlike zeolites Y and L). By using energy minimization calculations, it was not possible to determine relative orientation of the cobalt complex structure-directing agent inside the pores.

Acknowledgment. C.C.F., M.E.D., K.B., and R.F.L. are grateful to Chevron Research and Technology for financial support. K.B. was partially supported by NSF for this investigation. R.F.L. is grateful to the University of Delaware Research Foundation for financial support. M.T. acknowledges support from the National Center for Electron Microscopy at Lawrence Berkeley Laboratory through a NCEM/DOE fellowship. We thank the W.M. Keck Polymer Morphology Laboratory for use of microscopy facilities. We acknowledge T. Vogt and D. E. Cox for assistance in collecting the synchrotron data. The XRD data were collected at X7A beam line, National Synchrotron Light Source, Brookhaven National Laboratory, which is supported by the Department of Energy, Division of Materials Sciences and Division of Chemical Sciences.

Supporting Information Available: TEM of calcined UTD-1, illustration of intergrowths of poymorphs A and C, simulation of XRD patterns of polymorphs A and C, comparison of experimental and calculated XRD patterns of a 50% intergrowth of polymorphs C and D and input files for the program DIFFaX (15 pages). See any current masthead page for ordering and Internet access instructions.

JA9708528